5318–5326 *Nucleic Acids Research, 1998, Vol. 26, No. 23*

RNA structure adjacent to the attenuation determinant in the 5′-non-coding region influences poliovirus viability

Stacey R. Stewart and Bert L. Semler*

Department of Microbiology and Molecular Genetics, College of Medicine, University of California, Irvine, CA 92697, USA

Received August 28, 1998; Revised and Accepted October 13, 1998

ABSTRACT

In attenuated Sabin strains, point mutations within stem–loop V of the 5′-non-coding region (NCR) reduce neurovirulence and cell-specific cap-independent translation. The stem–loop V attenuation determinants lie within the highly structured internal ribosome entry site. Although stem–loop V Sabin mutations have been proposed to alter RNA secondary structure, efforts to identify such conformational changes have been unsuccessful. A previously described linker-scanning mutation (X472) modified five nucleotides adjacent to the attenuation determinant at nt 480 [for poliovirus (PV) type 1]. Transfection of X472 RNA generated only pseudo-revertants in HeLa (cervical carcinoma) or SK-N-SH (neuroblastoma) cells. Pseudo-revertants from both cell types contained nucleotide changes within the X472 linker. In addition, some neuroblastoma-isolated revertants revealed second site mutations within the pyrimidine-rich region located ~100 nt distal to the original lesion. Enzymatic RNA structure probing determined that the X472 linker substitution did not disrupt the overall conformation of stem–loop V but abolished base pairing adjacent to the attenuation determinant. Our analyses correlated increased base pairing proximal to the stem–loop V attenuation determinant with growth of X472 revertant RNAs (measured by northern blot analysis). Potential roles of second site mutations in the pyrimidine-rich region are discussed. In addition, our enzymatic structure probing results are shown on a consensus secondary structure model for stem–loop V of the PV 5′-NCR.

INTRODUCTION

Poliovirus (PV) primarily infects the primate alimentary tract and, therefore, is classified as an enterovirus. However, in ~1% of humans infected with PV, the neurovirulent phenotype of PV is expressed, resulting in paralytic poliomyelitis (1). Repeated passage of the three PV strains in animals and cultured cells generated the corresponding attenuated vaccine strains (Sabin types 1–3) (2). The improved ability of these PV variants to grow in non-nervous tissue compromised their ability to grow in the nervous system, as demonstrated by the decreased neurovirulence of these strains in monkeys (2).

Previous studies sought to identify which nucleotide changes in the attenuated Sabin genomes contributed to the transformation from neurovirulent to attenuated growth phenotypes in primates (reviewed in 3). One approach was to look at the reverse situation: which nucleotide reversions could restore neurovirulence to the attenuated strains? Sequence analysis of strains isolated from vaccine-associated poliomyelitis cases identified a critical residue at position 472 in the 5′-non-coding region (NCR) of Sabin type 3 (4). In the 12 cases investigated, all of the PV3 sequences showed reversion from a uridine to the wild-type cytidine. The importance of this nucleotide was further established by neurovirulence tests in monkeys, which showed that the nt 472 (U→C) transition correlated with an increase in neurovirulence (4). Following vaccination of human infants with Sabin types 1–3, RNA isolated from excreted virus showed a strong selection for reversions at similar positions in Sabin type 1 (nt 480), Sabin type 2 (nt 481) (5) and Sabin type 3 (nt 472) (4).

How do nucleotide changes in the Sabin strains reduce neurovirulence and, in particular, how do point mutations in the 5′-NCR at nt 480 (PV1), nt 481 (PV2) and nt 472 (PV3) contribute to defective growth in the nervous system? To elucidate the stage of the PV life cycle affected by genetic alterations in the Sabin genomes, Krebs-2 and rabbit reticulocyte lysates were used to measure *in vitro* translation levels of wild-type and mutated PV RNAs (6). Cell-free translation reactions programmed with virion RNAs from attenuated PV1 and PV3 translated less efficiently *in vitro* than the corresponding neurovirulent strains. Each of the 10 mutations in Sabin type 3 were investigated in the context of the wild-type PV3 genome for a potential contribution to the translation defect (7). Only the (C→U) mutation at nt 472 reduced *in vitro* translation in Krebs-2 extracts, thus drawing a connection between the mutations that affected PV neurovirulence (discussed above) and translation. Additional evidence for the role of nt 472 in neurotropism and translation came from cell culture studies with a virus harboring a genomic change only at nt 472 (8). PV3 containing the nt 472 mutation showed a 10-fold reduction in growth in SH-SY5Y (neuroblastoma) cells, but replicated to near wild-type levels in HeLa (cervical carcinoma) cells. This reduction in growth was

*To whom correspondence should be addressed. Tel: +1 949 824 7573; Fax: +1 949 824 8598; Email: blsemler@uci.edu

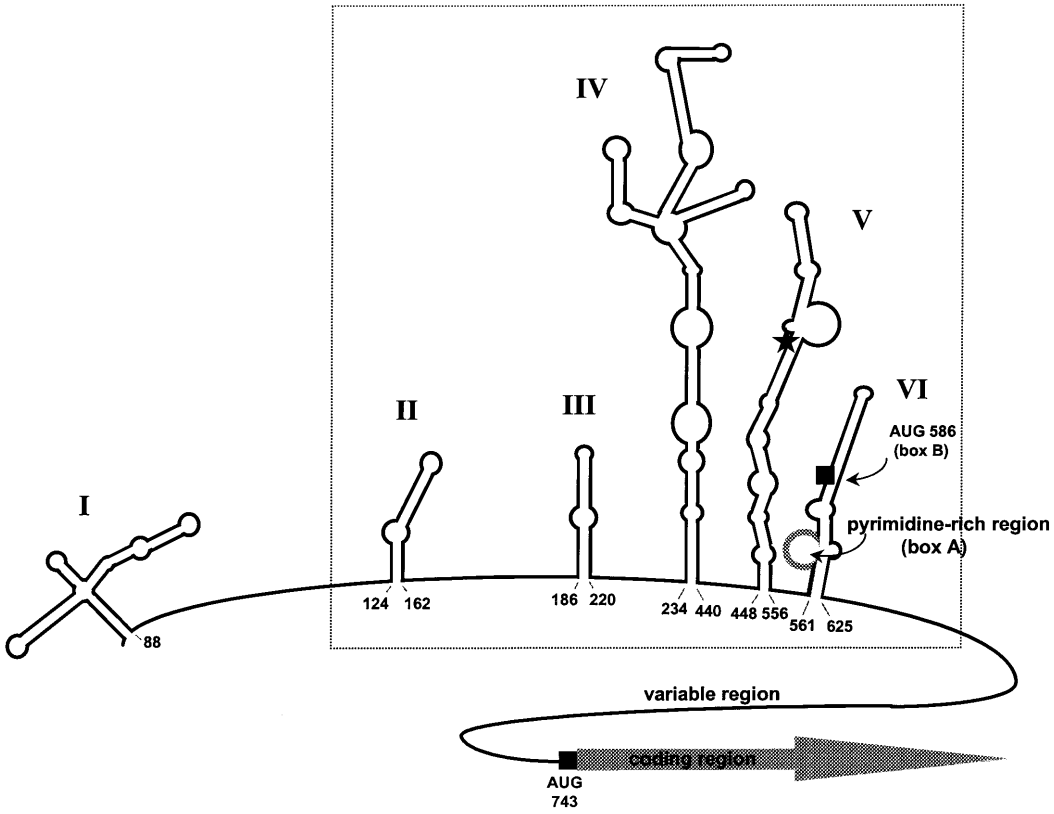

Figure 1. Predicted RNA secondary structure of the PV 5′-NCR. Stem–loops II–VI have been shown to form the internal ribosome entry site (IRES, boxed region). Sequences important for translation include the pyrimidine-rich region (box A) and AUG(586) (box B); AUG(743) initiates translation of the PV polyprotein. The attenuation determinant in stem–loop V is indicated by a star. Numbering refers to PV type 1 sequences.

due, at least in part, to a translation defect. Collectively, these and other studies indicate that the mutation at nt 472 in PV3 (and corresponding nucleotides in PV1 and PV2) has a function in neurotropism and translation of PV.

The lack of a 7-methylguanosine cap (9–11) and long length of the PV 5′-NCR (12) indicated that the genomic RNA was not translated using cap-dependent translation. Using a bicistronic construct in which the second cistron was preceded by the PV 5′-NCR, Pelletier and Sonenberg (13) demonstrated that the PV 5′-NCR initiated internal ribosome entry to the mRNA. It was possible, therefore, that point mutations in the Sabin 5′-NCRs could alter a protein binding site(s) and/or could disrupt higher order RNA–RNA interactions important for recruiting ribosomes to PV mRNA. Evans *et al.* (4) suggested that the nucleotide change at 472 in Sabin type 3 RNA altered the computer predicted secondary structure of the wild-type PV3 5′-NCR. However, the structure predictions in Evans *et al.* (4) are in disagreement with more comprehensive studies which take into consideration phylogenetic base pairing conservation and physical RNA secondary structure analyses (14–16). Based on these more recent RNA structure studies, the ~750 nt 5′-NCRs of PV1–3 were predicted to form six stem–loop structures (I–VI; Fig. 1). The strongly attenuating mutations in the 5′-NCRs of the Sabin strains lie in stem–loop V at positions predicted to base pair in wild-type sequences. Pilipenko *et al.* (14) investigated the possibility that the change from a C-G base pair to a weaker U-G interaction at nt 472 in Sabin type 3 RNA altered RNA secondary structure. Chemical and enzymatic methods of RNA structure probing were unable to identify any significant change in base pairing at, or adjacent to, nt 472 (Sabin type 3) compared with wild-type PV3 RNA (14).

In light of the above findings, we were intrigued by a previously described linker-scanning mutation (X472) in which a *Xho*I restriction site replaced wild-type sequences adjacent to the major attenuation determinant (nt 480) in stem–loop V of PV1 RNA (17,18). RNA harboring the X472 mutation was quasi-infectious because transfection of *in vitro* transcribed X472 RNA never yielded virus with RNA that retained the original stem–loop V lesion. However, two pseudo-revertants (PVX472-R1H and PVX472-R2H) were recovered from HeLa cells transfected with X472 RNA and, following sequencing of the viral RNAs, revealed nucleotide changes within the *Xho*I linker sequence (18). Translation of PVX472-R1H and PVX472-R2H was more defective than Sabin type 1 in *in vitro* rabbit reticulocyte lysate translation reactions supplemented with neuroblastoma cell extracts and in neuroblastoma cell infections (18). However, PVX472-R1H, PVX472-R2H and Sabin type 1 showed translation levels similar to wild-type PV1 in *in vitro* translation reactions in the presence of HeLa cell extract or in HeLa cells infected with the viruses (18). One interpretation of these findings is that the lesions in R1H and R2H RNAs exacerbate the defective interaction caused by the stem–loop V point mutation in Sabin type 1 RNA. Results described here indicate that different nucleotide changes compensated for the X472 lesion when

revertants were isolated from SK-N-SH (neuroblastoma) cells compared with reversions originating from HeLa cell selection. Two X472 revertants from SK-N-SH cells (X472-R4N and X472-R5N) contained seven nucleotide changes in the conserved pyrimidine-rich region, which lies ~100 nt from the original stem–loop V lesion.

RNA structure probing was used to investigate potential RNA structure changes that may have been introduced by the X472 lesion and compensatory mutations. Results from this analysis indicated that the X472 linker-scanning mutation decreased base pairing adjacent to the attenuation determinant in stem–loop V. RNAs isolated from pseudo-revertants derived from both HeLa and SK-N-SH cells showed increased base pairing within the X472 lesion, indicating the importance of RNA structure near the attenuation determinant for viability in both cell types. RNA structure changes in the revertant RNAs correlated with a restoration of virus growth, as measured by northern blot analysis. Taken together, these findings indicate that the structure and, perhaps, sequences near the attenuation determinant in stem–loop V of the 5′-NCR affect PV viability. Possible mechanisms by which nucleotide changes in the pyrimidine-rich region could compensate for the X472 lesion are discussed.

MATERIALS AND METHODS

In vitro RNA synthesis

Full-length RNAs used for transfection experiments were generated using MAXIscript (Ambion) starting with ~1 µg of *Eco*RI-linearized plasmid/reaction. Since larger quantities of RNA were needed for RNA structure probing analysis, MEGA-shortscript (Ambion) was used for *in vitro* transcription of 1 µg of pGS-FG (or mutated constructs) linearized with *Bsa*BI (at nt 605). RNAs generated for use in structure probing assays were phenol/chloroform extracted, ethanol precipitated, resuspended in DEPC-treated water and stored at –70°C.

Isolation of X472 revertants from SK-N-SH (neuroblastoma) cells

In vitro transcription of the plasmid pT7PVX472 (17) generated genomic-length PV1 RNA harboring a linker-scanning mutation at nt 472. SK-N-SH monolayers were transfected with the X472 RNA using DEAE–dextran as described (19), except that the cells were overlaid with DME plus 20% fetal calf serum (FCS). Transfected cells were incubated at 37 or 39°C for 1 day and, following incubation, each plate was scraped with a sterile scraper. Cells and medium from each plate were placed in cryovials and freeze–thawed five times to release intracellular viruses. The lysates generated as such were used to infect SK-N-SH monolayers at 10^{-1}–10^{-4} dilutions. Viruses were adsorbed to SK-N-SH cells at room temperature for 30 min with occasional rocking. DME supplemented with 20% FCS was added to the cells and incubated at 37 or 39°C under semi-solid agarose until plaques were visible on the monolayers (2 days). Plaques were isolated using a Pasteur pipette, placed into Eppendorf tubes containing 1 ml of PBS and freeze–thawed. Virus clones were expanded into passage one (P1) or passage two (P2) stocks by infecting SK-N-SH monolayers with virus from the plaque isolate or P1 stock, respectively. Following incubation at 37 or 39°C for ~12 h, lysates were freeze–thawed five times.

RNA sequence analysis

Total cellular RNA was isolated (20) from SK-N-SH cells infected with revertant viruses. Aliquots of 3 pmol of L164–primer (5′-TCAGAGTGAAAGTGGCCT-3′), 5 µg of RNA and DEPC-treated water (to bring the volume up to 10 µl) were boiled for 2 min. The samples were allowed to cool to room temperature, centrifuged and placed on ice. cDNAs were generated using AMV reverse transcriptase (US Biochemical) at 50°C to minimize RNA secondary structure. Extension reactions were performed for 5 min in the presence of 1× AMV reverse transcriptase buffer (50 mM Tris–HCl, pH 8.3, 8 mM $MgCl_2$, 50 mM NaCl, 1 mM DTT), labeling mix (7.5 µM dGTP, dCTP and dTTP), 5 µCi [^{35}S]dATP and DEPC-treated water (to bring the final volume up to 20 µl). Aliquots of 4 µl of each ddNTP termination mix (for each NTP, 50 mM NaCl, 40 µM ddNTP, 160 µM dNTP, 200 µM each of the other three dNTPs) were pre-heated to 50°C for 1 min before addition of 4 µl of the extension reaction. Incubation was continued at 50°C for 10 min followed by the addition of 4 µl of stop solution (95% formamide, 20 mM EDTA, 0.05% bromophenol blue, 0.05% xylene cyanol). Samples were boiled for 3 min, cooled on ice, centrifuged and separated on a pre-warmed 8.5% polyacrylamide gel containing 7 M urea.

Cloning X472 reversion mutations into plasmids for expression of stem–loops V and VI of the 5′-NCR or full-length PV1 genomic sequences

RNA was isolated as described (20) from SK-N-SH cells infected with wild-type or revertant viruses. One microgram of total RNA was used for reverse transcription (RT) and amplification using PCR in a Perkin-Elmer DNA Thermo cycler 480. RT–PCR reactions also contained 0.2 mM dNTPs, 24 pmol of primers AH412+ (5′-GGTGTGAAGAGCCTATTGAG-3′) and L392– (5′-GTGCGCCCACTTTCTGTGAT-3′), 1 U of DeepVent DNA polymerase (NE Biolabs), 1× ThermoPol buffer, 10 U of AMV reverse transcriptase, 20 U of RNasin RNase inhibitor (Promega) and DEPC-treated water to bring the reaction volume up to 50 µl. Prior to the addition of DNA polymerase, reverse transcriptase and RNasin, the reactions were boiled for 2 min and cooled on ice. The remaining reaction components were added and the mixtures were incubated in the thermocycler for 30 min at 50°C followed by 25 cycles of 1 min at 94°C, 1 min at 55°C and 2 min at 72°C. *Bsm*I and *Msc*I digests were performed on the above RT–PCR products, pT7-PV1 (a plasmid containing the full-length PV1 genome under a T7 RNA polymerase promoter) (17) and pGS-FG (a plasmid containing PV1 nt 445–627 preceeded by 16 non-viral nucleotides and a T7 RNA polymerase promoter). 5′-Terminal phosphate groups were removed from vector fragments using calf intestinal alkaline phosphatase (Promega). T4 DNA ligase (US Biochemical) was used to ligate each of the *Bsm*I–*Msc*I fragments into the phosphatase-treated vectors. The resulting clones were verified by DNA sequencing with Sequenase v.1.0 (US Biochemical). Note that X472-R1H, X472-R4N, etc. refer to viruses and R1H, R4N, etc. designate RNAs harboring the stem–loop V and/or VI lesions.

Growth analysis of revertants using northern blot assay

In vitro transcribed RNAs were quantitated on a 1% agarose gel and ~1 µg of each RNA was transfected into HeLa cell

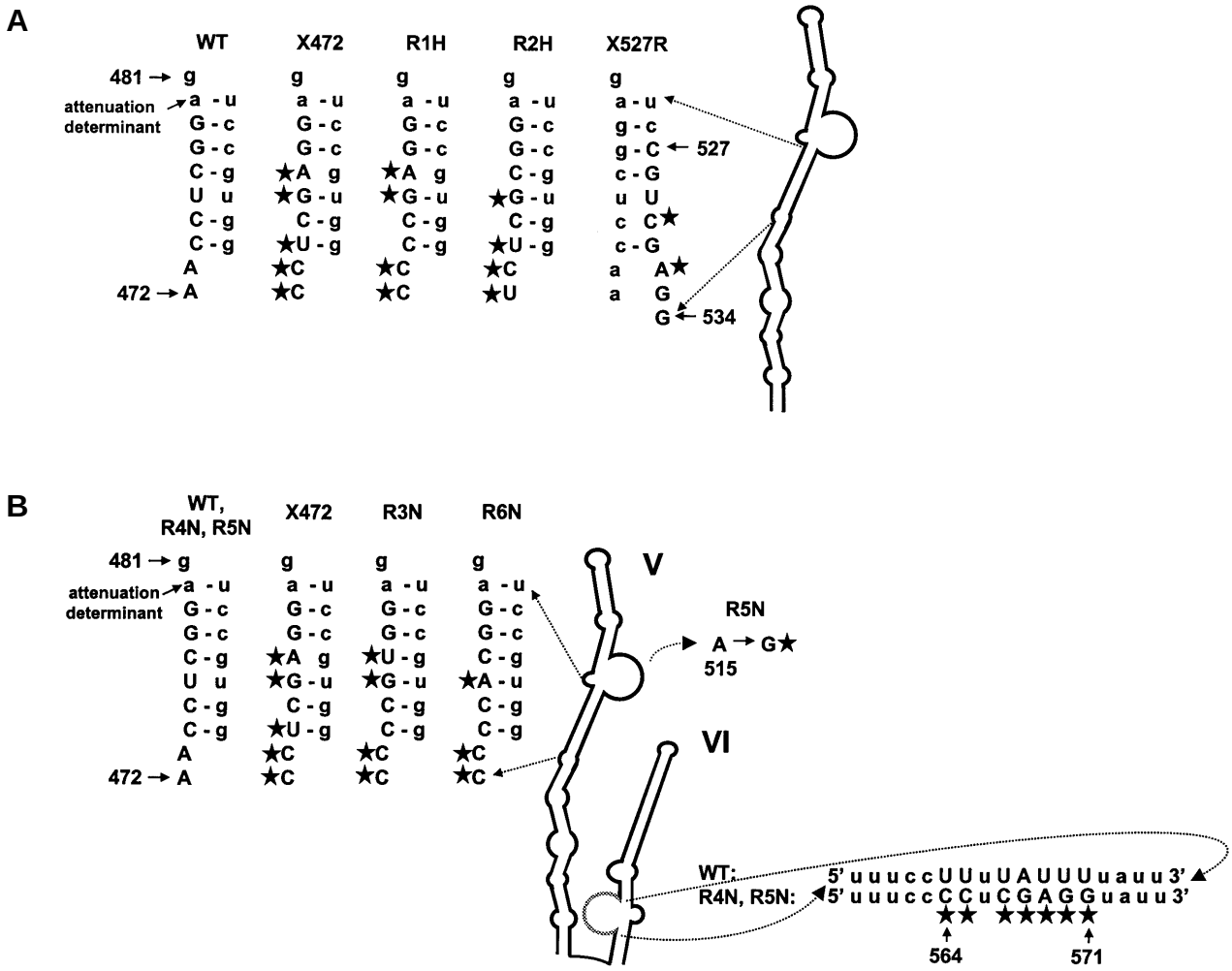

Figure 2. Sequences of wild-type, X472 and X472 revertant RNAs from (**A**) HeLa cells and (**B**) SK-N-SH (neuroblastoma) cells. Stem–loop outlines depict the regions of stem–loops V and VI that are shown in greater detail for sequence analysis. The *Xho*I cassette in X472 RNA extends between nt 472 and 479 and is indicated in upper case. Upper case letters are also used to highlight second site reversions at nt 515 (R5N) and in the pyrimidine-rich region (R4N and R5N). Nucleotides that differ from wild-type residues are indicated by stars.

monolayers (19). Cells were overlaid with 5 ml of DME supplemented with 10% NCS and incubated for the indicated times at 37°C. RNA harvests were generated using RNA STAT-60 (Leedo Medical Laboratories). Aliquots of 5 µg of total RNA were glyoxal-treated (21) for each time point. Hybridization and washing conditions were as described (19).

RNA secondary structure probing using primer extension

Structure probing was performed essentially as described (22). Approximately 0.5 µg of RNA was incubated with RNase for 10 min at room temperature in 0.7× TMK buffer (30 mM Tris, pH 7.4, 10 mM $MgCl_2$, 270 mM KCl) or in the presence of varying concentrations of KCl (as described in Results) plus 40 µg of tRNA and 18 mM β-mercaptoethanol. RNases were used in two dilutions as follows: RNase V_1, 7 or 0.7 U; RNase T_1, 20 or 2 U; RNase U_2, 2 or 0.4 U; RNase Bc, 10 or 2 U. Extension reactions were performed with ~10^6 c.p.m. [γ-^{32}P]ATP 5′-end-labeled primer (~2 pmol) SS601– (5′-CTGTGATTGTCACCA-TAAGC-3′), which is complementary to PV nt 582–601.

RESULTS

Secondary structure probing of revertant RNAs isolated from HeLa cells

Stem–loop V RNA sequences from wild-type PV1, the original linker-scanning mutation (X472) and the two revertants isolated from HeLa cells (X472-R1H and X472-R2H) are shown in Figure 2A. Within the 8 nt *Xho*I linker in X472, 5 nt differ from wild-type sequences and would be expected to disrupt base pairing in the stem adjacent to the attenuation determinant at nt 480. Reversion mutations in R1 and R2 RNAs are located within the linker-scanning mutation beginning at nt 472. These pseudo-reversions could partially restore wild-type base pairing in the stem region with the exception of the C→U reversion at nt 472

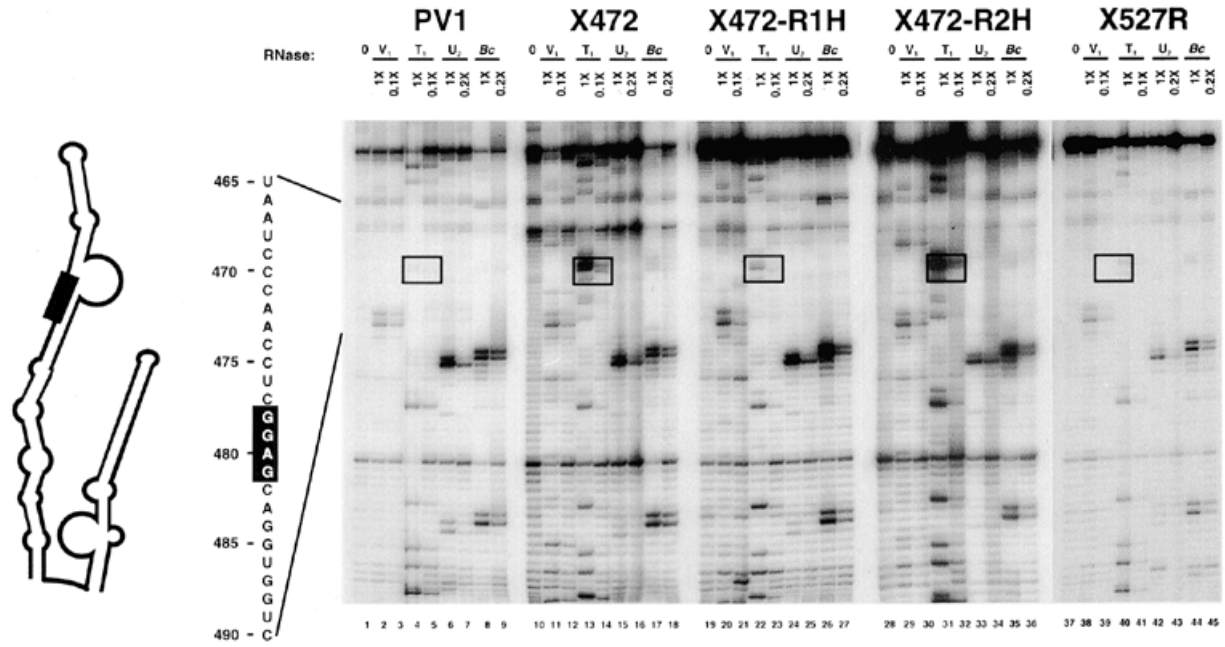

Figure 3. Structure probing near the stem–loop V attenuation determinant of RNAs from wild-type, X472 and revertants from HeLa cells. Enzymes were used in two dilutions (Materials and Methods) to ensure partial digestion conditions. Note that the full-length undigested RNAs are not shown at the top of the autoradiogram. RNase T_1-sensitive guanosines (in X472 and R2H) are indicated by boxes in the structure probing results and in the diagram of stem–loops V and VI at the left. The specificities and concentrations of enzymes used to derive data shown in Figures 3–5 and 7 are as follows: RNase V_1, dsRNA, 7 or 0.7 U; RNase T_1, Gp↓N, 20 or 2 U; RNase U_2, Ap↓N, 2 or 0.4 U; an RNase isolated from *B.cereus* (RNase *Bc*), Up↓N and Cp↓N, 10 or 2 U.

in R2; this reversion is located in a predicted single-stranded loop in wild-type stem–loop V.

Enzymatic structure probing was employed to determine stem–loop V secondary structures of X472, R1H, R2H and X527R RNAs in comparison with wild-type RNA (Figs 3 and 4). X527R RNA (Fig. 2A) was included as a control because it contains a reversion from a linker-scanning mutation that was predicted to be on the opposite side of the stem from the X472 mutation. RNases V_1 (dsRNA), T_1 (Gp↓N) and U_2 (Ap↓N) and an RNase isolated from *Bacillus cereus* (herein referred to as RNase *Bc*) (Up↓N and Cp↓N) were used for partial digestion of wild-type or mutated RNAs. Cleavage assays were performed on *in vitro* transcribed RNAs generated from plasmids containing reconstructed cDNA sequences of stem–loops IV–VI (R1H, R2H and X527R) or stem–loops V and VI (wild-type and all other mutated constructs). Since salt concentrations can influence higher order RNA conformations, enzymatic cleavage was conducted in TMK buffer (Materials and Methods) containing final concentrations of 0, 50, 100 and 200 mM KCl. Changes in KCl concentrations did not alter the pattern of enzymatic cleavage; however, cleavage by RNase V_1 was enhanced at higher concentrations of KCl, denoting the stabilization of helical structures in the presence of salt (data not shown). A final concentration of 180 mM KCl, which is within the range of intracellular salt concentrations, was used in the secondary structure probing shown here. Wild-type RNAs containing stem–loops IV–VI, V and VI or V and the 5′-half of VI produced nearly identical digestion patterns (data not shown), indicating that stem–loop V was capable of folding independently of surrounding sequences. RNAs containing stem–loops IV–VI (R1H, R2H and 527R RNAs) or V and VI (all other RNAs) were truncated within stem–loop VI because the high degree of base pairing in stem–loop VI severely inhibited the primer extension reaction (data not shown). Primer extension was performed with a 5′-^{32}P-end-labeled deoxyoligonucleotide complementary to sequences internal to stem–loop VI. Products of the primer extension reactions are 1 nt shorter than the corresponding position in the sequencing ladder due to the removal of the 3′-proximal ribonucleotide during enzymatic cleavage.

Figure 3 shows the pattern of enzymatic digestion for the 5′-side of stem–loop V of wild-type, X472 and revertant RNAs isolated from HeLa cells. The boxed regions in the autoradiographs denote the guanosine residues with increased RNase T_1 sensitivity in the X472 RNA (Fig. 3, lanes 13 and 14) compared with the corresponding nucleotides in wild-type RNA (Fig. 3, lanes 4 and 5). Cleavage at the guanosine residues in X472 RNA indicated that the presence of the linker-scanning mutation from nt 472 to 479 resulted in a decrease in base pairing at nt 478, 479 and 481 in the X472 RNA. Note that G478, G479 and G481 were present in all of the RNA constructs shown (Fig. 2A); hence, differences in sensitivity to RNase T_1 were not due to sequence changes at the sites of enzymatic cleavage. R1H RNA (Fig. 3, lanes 22 and 23) showed RNase T_1 sensitivity intermediate to that observed for wild-type and X472 sequences. RNase T_1 digestion of R2H RNA (lanes 31 and 32) more closely resembled the cleavage pattern of X472 RNA. Guanosine residues in the same position in X527R RNA showed limited cleavage by RNase T_1, closely matching the digestion pattern observed for wild-type sequences.

RNase digestion of the 3′-side of stem–loop V is shown in Figure 4. There was a slight increase in the sensitivity of nt 528, 530 and 531 to RNase T_1 digestion in X472, R1 and R2 RNAs compared with the corresponding sequences in wild-type and

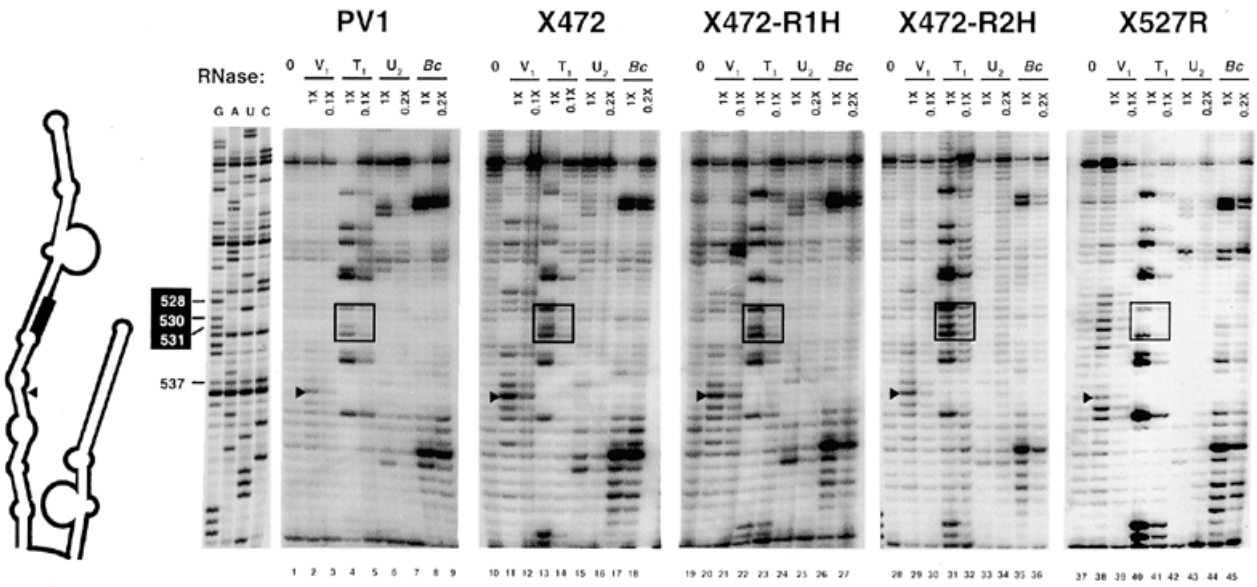

Figure 4. Secondary structure analysis of RNAs from wild-type, X472 and revertants from HeLa cells at positions predicted to base pair with sequences near the stem–loop V attenuation determinant. Boxed regions in the structure probing autoradiograms and the stem–loop V illustration denote RNase T_1-hypersensitive guanosines (in X472, R1H and R2H). Arrowheads indicate RNase V_1 cleavage at nt 537. Note that positions cleaved by RNases migrate 1 nt further in the structure probing data compared with the sequencing ladder; this is due to RNase-mediated removal of the 3′-terminal nucleotide, which is then not present in the template RNAs used for primer extension. The full-length undigested RNAs are not shown at the top of the autoradiogram.

X527R sequences (compare the intensity of the RNase T_1-sensitive sites in the boxed region with those sites above and below the box for each RNA). Increased RNase T_1 cleavage of the (boxed) guanosines in X472, R1H and R2H RNAs (Fig. 4) was in accordance with the predicted location of these nucleotides on the opposite side of the stem structure from nt 478, 479 and 481 (Fig. 2A). Results from structure probing of the 5′- (Fig. 3) and 3′-sides (Fig. 4) of stem–loop V suggested that sequences adjacent to the two (boxed) RNase T_1-sensitive regions in X472 RNA were base paired in wild-type RNA and that the mutations in X472, R1H and R2H RNAs resulted in a partial unfolding of this domain. In addition, a slight increase in RNase V_1 cleavage of X472, R1H and R2H RNAs was observed at C537 compared with the same nucleotide in wild-type or X527R sequences (Fig. 4). Increased RNase V_1 cleavage at C537 in the mutated RNAs does not suggest that a different conformation is formed in this region of stem–loop V, but that the double-stranded character present in the wild-type and X527R RNAs is further stabilized in the X472 mutated and revertant stem–loop V. With the exception of the boxed guanosine residues (Figs 3 and 4) and C537 (Fig. 4), the sensitivities of wild-type and mutated RNAs to RNases V_1, T_1, U_2 and *Bc* were very similar. Therefore, it appeared that the X472 mutation did not result in misfolding of stem–loop V; rather, it affected the RNA structure by decreasing base pairing in the vicinity of the *Xho*I linker.

Secondary structure probing of revertant RNAs isolated from neuroblastoma cells

Since the attenuation determinant in stem–loop V of PV RNA influences virus growth in the mammalian nervous system, it was of interest to determine whether different X472 reversion mutations would be generated during an infection of neuroblastoma cells. To generate potential revertants, *in vitro* transcribed full-length genomic PV RNA containing the X472 linker-scanning mutation (Fig. 2B) was transfected into 12 SK-N-SH (neuroblastoma) monolayers; six were incubated at 37°C and the other six were incubated at 39°C. Revertant viruses were isolated as described in Materials and Methods. Following direct sequencing of stem–loops V and VI of the viral RNAs, the revertant viruses could be divided into four groups, which are represented by X472-R3N, X472-R4N, X472-R5N and X472-R6N. Stem–loop V and pyrimidine-rich region sequences of these revertants are shown in Figure 2B. RNAs isolated from X472-R3N and X472-R6N viruses contained pseudo-reversions within the linker-scanning mutation in stem–loop V. A complete reversion from the X472 linker-scanning mutation to wild-type stem–loop V sequences was observed in R4N and R5N RNAs; however, both isolates contained seven nucleotide changes in the conserved pyrimidine-rich region located ~100 nt distal to the original lesion in stem–loop V. The seven pyrimidine-rich region mutations were found in one plaque isolate from the 37°C incubation and in eight isolates generated from four different transfected monolayers incubated at 39°C. In addition, R5N RNA harbored an A515→G515 transition (located in stem–loop V; Fig. 2B). The point mutation at nt 515 in R5N was found in only one of the plaque isolates containing the pyrimidine-rich region mutations and, therefore, may be a non-deleterious random mutation or may play a role in the growth phenotype of X472-R5N.

Secondary structure probing was performed on stem–loop V RNA from wild-type PV1, X472 and revertants isolated from neuroblastoma cells (Fig. 5). As observed in Figure 3, X472 RNA (Fig. 5, lanes 13–14) showed an increased sensitivity to RNase T_1 digestion at nt 478, 479 and 481 compared with the very low level of cleavage in PV1 RNA (Fig. 5, lanes 4–5). R3N was the only RNA containing revertant sequences which showed RNase T_1

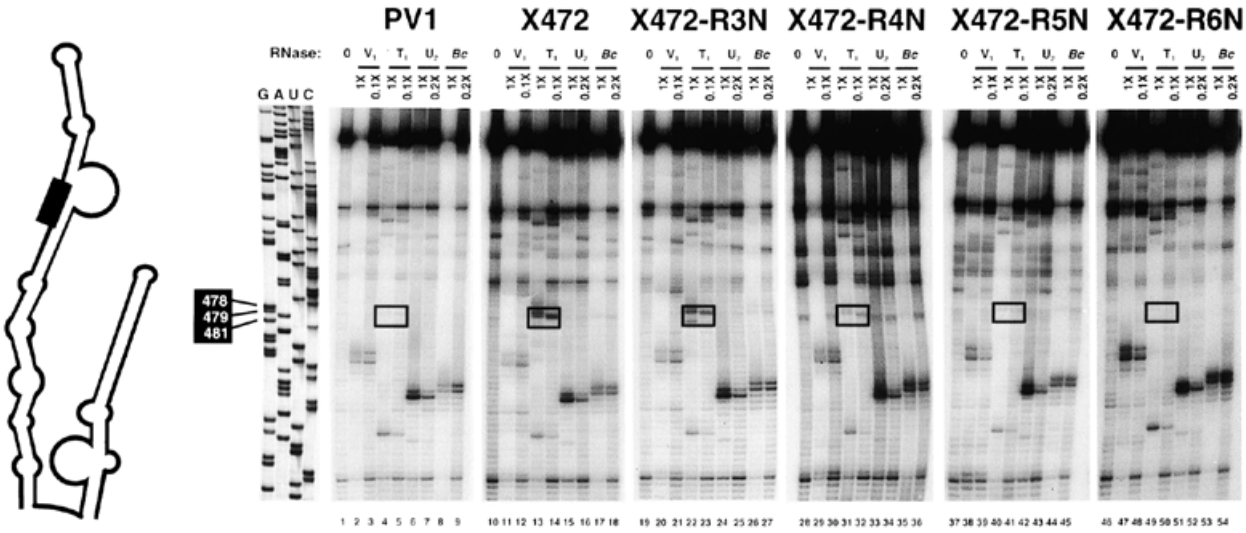

Figure 5. Stem–loop V secondary structure probing of RNAs from wild-type, X472 and X472 revertants isolated from SK-N-SH cells. RNase T_1-sensitive guanylate residues at nt 478, 479 and 481 (X472 and R3N) are indicated by boxes in the stem–loop V diagram and data shown on the right. The top of the autoradiogram shows the full-length undigested RNAs.

cleavage comparable with the digestion pattern of X472 RNA (Fig. 5, lanes 22–23). In enzymatic digests performed on the opposite side of the helix, X472 and R3N showed higher levels of RNase T_1 scission at G528, G530 and G531 than wild-type or the other revertant RNAs (data not shown). Thus, X472 and R3N RNAs demonstrated increased single-stranded character adjacent to the stem–loop V attenuation determinant, whereas wild-type, R4N, R5N and R6N RNAs exhibited base pairing within this region.

Northern blot analysis of reconstructed RNAs containing stem–loop V and pyrimidine-rich region reversion mutations

To ensure that the identified reversion mutations in X472-R3N, X472-R4N, X472-R5N and X472-R6N were responsible for restoring growth to the X472 mutated RNA, stem–loops V and VI from the revertant RNAs were reverse transcribed and amplified using PCR (Materials and Methods). The resulting DNA fragments were cloned into a plasmid containing the full-length PV cDNA (pT7-PV1). *In vitro* transcribed RNAs generated from these reconstructed plasmids, therefore, contained mutations only in stem–loops V and VI. As a measure of viability, northern blot analysis was performed on RNA isolated from HeLa cells transfected with wild-type, X472 mutated or revertant RNAs (Fig. 6). Transfections were performed in HeLa cells due to the increased RNA yields obtained from this cell type compared with SK-N-SH cells. X472 RNA did not replicate (lanes 6–9); however, wild-type and all of the revertant RNAs replicated to detectable levels by the 18 h time point. R6N appeared to replicate more efficiently than wild-type RNA, as indicated by the appearance of viral RNA at the 14 h time point. Results from the northern blot analysis demonstrated that the reversion mutations in stem–loop V and the pyrimidine-rich region were responsible for restoring viability to the X472 mutated RNA and that the neuroblastoma-isolated revertants were also viable in HeLa cells.

Sequence analysis of pyrimidine-rich region reversions in R4N and R5N

Do the seven nucleotide changes in the pyrimidine-rich region interact with the original X472 lesion? Since the second site mutations from nt 564 to 571 generated a *Xho*I site, it was possible that the pyrimidine-rich mutations could have base paired with the *Xho*I sequence at nt 472. In order for this base pairing to occur, the original X472 linker-scanning mutation would need to be present on the same RNA as the pyrimidine-rich region mutations. To investigate whether the stem–loop V and pyrimidine-rich region mutations coexisted, RNA was isolated from the original X472 RNA transfection harvests, the plaque isolates and the passage 2 (P2) virus stocks for X472-R4N and X472-R5N. RNA from the plaque isolates was directly sequenced, whereas RNA from the transfection and P2 harvests was too low in concentration to directly sequence, so this RNA was reverse transcribed and PCR-amplified prior to DNA sequencing of the PCR products. Results from these analyses indicated that the two sequences could not have base paired; in particular, uridines at nt 570 and 571 were mutated to guanosines in viruses isolated from the transfection harvests. Concurrently, the predicted base pairing partners of residues 570 and 571 (C472 and C473) reverted to adenosines, abolishing potential C472-G571 and C473-G570 base pairing. Thus, it remains to be determined whether the pyrimidine-rich region mutations interact with a protein or RNA sequence of cellular or viral origin. Experiments in our laboratory are currently underway to elucidate how the second site mutations in the pyrimidine-rich region augment the growth of X472-R4N and X472-R5N and whether the nature of the interaction differs between the intracellular environments of neuroblastoma and HeLa cells.

DISCUSSION

Mutations that significantly contribute to PV neurotropism were previously localized to what is now referred to as stem–loop V in

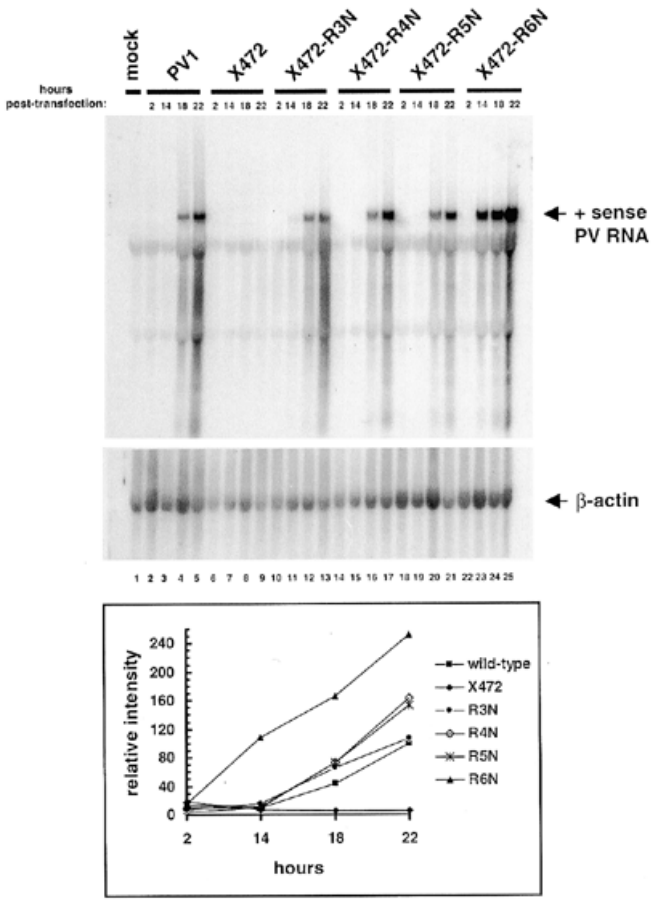

Figure 6. Northern blot analysis of wild-type or mutated RNAs transfected into HeLa cells. The ~7.5 kb message-sense PV genome is indicated in the top panel. β-Actin mRNA levels were probed on the same blot (lower) to measure differences in gel loading. Positive-sense PV RNA levels were normalized to β-actin mRNA levels and a graph representing the results is shown at the bottom. The peak concentration of wild-type RNA (22 h post-transfection) was arbitrarily set at 100%. RNA levels were quantitated on scanned images from a Hewlett Packard ScanJet IIcx scanner using SigmaScan/Image measurement software.

the 5′-NCR (Fig. 1) of the Sabin strains (4,5,23,24). The stem–loop V point mutation in each of the Sabin strains not only decreased neurotropism of viruses containing the mutated RNA sequence, but also reduced translation levels of the RNAs *in vitro* (6,7). Thus, PV neurotropism and translation appear to be interrelated, perhaps due to the involvement of a neuronal-specific factor in cap-independent translation of the PV genome. Furthermore, since nucleotide changes involved in neurovirulence reside in similar locations in stem–loop V of the Sabin strains 1–3, attenuated growth of these PV variants in the primate nervous system appears to be influenced by a common defective mechanism. The work presented here was aimed at testing the hypothesis that RNA sequences and structures adjacent to the attenuation determinant in stem–loop V of the 5′-NCR influence PV viability in mammalian cells.

Previous studies with the linker-scanning mutation X472 indicated that the sequence changes introduced adjacent to the attenuation determinant at nt 480 (PV1) resulted in a pseudo-infectious RNA, X472 (Fig. 2A; 17,18). One explanation for the lack of viability of this construct was that the X472 lesion resulted in the misfolding of stem–loop V and that the deleterious effects on viability were not due to primary and secondary structure changes specifically at the *Xho*I linker at nt 472. Alternatively, the X472 lesion may have affected only sequences and structures near the attenuation determinant in stem–loop V, allowing for the use of X472 and revertants in elucidating RNA sequence and structure determinants participating in translation and neurotropism of PV. Our results from enzymatic structure probing demonstrated that the X472 linker-scanning mutation opened up the helical conformation of stem–loop V at nt 478, 479 and 481 (surrounding the attenuation determinant at nt 480) and on the opposite side of the stem at nt 528, 530 and 531 (Fig. 7, green arrows). The nucleotide changes in X472 and the reversion mutations in stem–loop V lie between nt 472 and 477 (Fig. 7, green stars); therefore, differences in cleavage at G478, G479 and G481 were not due to sequence changes that would abolish RNase T_1 recognition. Although nt 537 was slightly sensitive to RNase V_1 in wild-type RNA, all of the mutated RNAs showed higher RNase V_1 cleavage at this position (Fig. 4 and data not shown). Perhaps opening up the neighboring helix at G528, G530 and G531 stabilized the base pairing at C537. RNase cleavage events in other regions of stem–loop V demonstrated that the X472 linker-scanning mutation did not result in global misfolding of stem–loop V (compare hypersensitive nucleotides in wild-type and mutated RNAs outside the boxed sequences in Figs 3–5). In particular, RNase V_1 cleavage sites conserved between X472, revertant and wild-type stem–loop V RNAs (Fig. 7, red arrows) indicated that the higher order stem–loop V conformation was retained in mutated constructs.

If secondary structure is the only determinant for viability of the X472 mutated RNA, then we would predict that second site mutations would also be observed on the opposite side of the helix. In fact, all of the stem–loop V reversion mutations were restricted to the X472 lesion on the 5′-side of stem–loop V, highlighting the importance of primary sequence within this region. Furthermore, R3N displayed single-stranded character in stem–loop V similar to X472 (Fig. 5), yet displayed an RNA replication phenotype similar to wild-type RNA (Fig. 6). R3N may contain sequence determinants that allowed for restored replication in the presence of decreased stem–loop V base pairing. U477 in R3N may be an example of such a sequence determinant. However, the uridine residue at nt 477 has not been examined by itself for a contribution to PV growth. At least two functions for sequence-specific determinants could explain these phenomena: (i) concomitant primary and secondary structure could form a protein-binding site that includes nt 472–481; (ii) in addition to interactions with nt 525–531 on the opposite side of the helix, nt 472–481 could interact with other viral or cellular RNA sequences. We do not have evidence to discriminate between these possibilities. Additional evidence supporting the importance of primary structure within the X472 lesion comes from nucleotide reversions that do not appear to participate in base pairing interactions. Two examples are A472 and A473 (Fig. 2B). Both of these nucleotides reverted from cytidine residues in X472 mutated RNA to the wild-type adenosine residues in R4N and R5N sequences, perhaps restoring the potential RNA–protein or RNA–RNA interactions just mentioned. Contrary to the other nucleotide changes introduced by the *Xho*I linker, G476 introduces a G-U base pair where bulged U residues are predicted to reside in wild-type RNA at nt 476 and 529 (Fig. 2A).

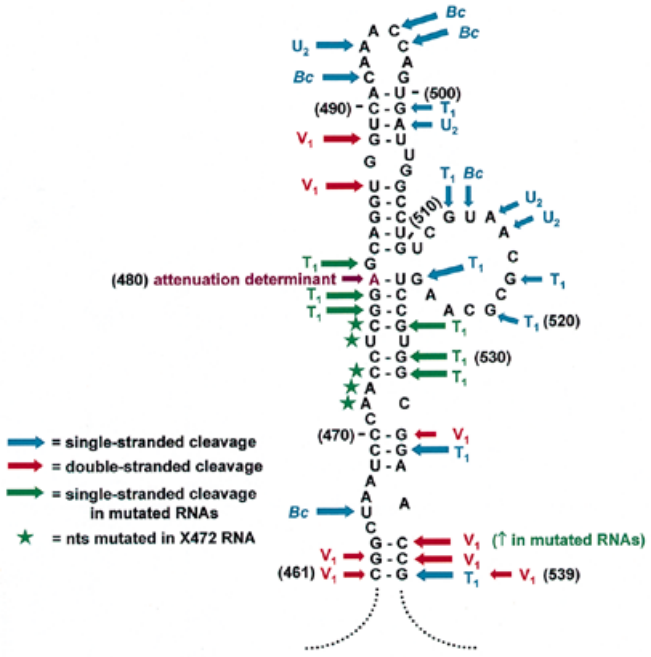

Figure 7. Secondary structure prediction of stem–loop V of the PV 5′-NCR. Red arrows (RNase V_1 cleavage of dsRNA) and blue arrows (RNases that recognize single-stranded residues) represent stem–loop V structure probing data derived from enzymatic digestion of wild-type PV1 RNAs containing either stem–loops V and VI or full-length genomic sequences (Figs 3–5 and data not shown). Longer arrows indicate increased RNA scission at the indicated nucleotide. The stem–loop V attenuation determinant is highlighted in purple. Nucleotides altered by the X472 linker-scanning mutation are indicated by green stars, and green arrows show RNase T_1-sensitive residues in X472 and some of the revertant RNAs.

Note that all of the revertants that retain cytidine residues at nt 472 and 473 have sequences capable of forming G-U or A-U base pairs at the predicted bulged U476. One possible explanation for this is that the presence of C472 and C473 allows base pairing with G530 and G531, and that this altered base pairing can be abolished by strengthening the interactions between adjacent nt 476 and 529. In the context of wild-type RNA sequences, the potentially single-stranded U476 and U529 may be structural elements of the stem–loop V attenuation determinant.

Previous efforts to correlate RNA conformational changes with the attenuation mutations in stem–loop V were unsuccessful (14). However, RNA structure analyses presented here indicate that primary and secondary structures adjacent to the attenuation determinant in stem–loop V of the 5′-NCR strongly influence PV viability in both HeLa and neuroblastoma cell lines. Undoubtedly, the five nucleotide changes in X472 RNA produced more structural changes than the point mutation in Sabin stem–loop V sequences, thereby making it possible to detect structural alterations in the X472 linker-scanning mutation that were too subtle to measure in Sabin RNAs. Although it is not known if RNA from Sabin strains exhibits a stem–loop V conformational change, it does appear that structural alterations adjacent to the attenuation determinant within stem–loop V affect PV growth. Whether the stem–loop V defect that contributes to the attenuation of Sabin strains is affecting the same mechanism modified by the X472 linker-scanning mutation remains to be determined.

ACKNOWLEDGEMENTS

We thank Hung Nguyen for technical expertise, Dr Suzanne Sandmeyer for helpful suggestions and Dr Louis Leong and Gwendolyn Jang for critical reading of the manuscript. S.R.S. was supported by a predoctoral training grant from the National Institutes of Health (AI07319). This work was supported by Public Health Service grants AI 26765 and AI 12387 from the National Institutes of Health.

REFERENCES

1 Minor,P.D. (1997) In Nathanson,N. (ed.), *Viral Pathogenesis*. Lippincott-Raven, Philidelphia, PA, pp. 555–574.
2 Sabin,A.B. (1965) *J. Am. Med. Assoc.*, **194**, 130–134.
3 Haller,A.A. and Semler,B.L. (1994) In McKendall,R.R. and Stroop,W.G. (eds), *Handbook of Neurovirology*. Marcel Dekker, New York, NY, pp. 481–491.
4 Evans,D.M., Dunn,G., Minor,P.D., Schild,G.C., Cann,A.J., Stanway,G., Almond,J.W., Currey,K. and Maizel,J.V. (1985) *Nature*, **314**, 548–550.
5 Minor,P.D. and Dunn,G. (1988) *J. Gen. Virol.*, **69**, 1091–1096.
6 Svitkin,Y.V., Maslova,S.V. and Agol,V.I. (1985) *Virology*, **147**, 243–252.
7 Svitkin,Y.V., Cammack,N., Minor,P.D. and Almond,J.W. (1990) *Virology*, **175**, 103–109.
8 La Monica,N. and Racaniello,V.R. (1989) *J. Virol.*, **63**, 2357–2360.
9 Fernandez-Munoz,R. and Darnell,J.E. (1976) *J. Virol.*, **18**, 719–726.
10 Hewlett,M.J., Rose,J.K. and Baltimore,D. (1976) *Proc. Natl Acad. Sci. USA*, **73**, 327–330.
11 Nomoto,A., Lee,Y.F. and Wimmer,E. (1976) *Proc. Natl Acad. Sci. USA*, **73**, 375–380.
12 Kitamura,N., Semler,B.L., Rothberg,P.G., Larsen,G.R., Adler,C.J., Dorner,A.J., Emini,E.A., Hanecak,R., Lee,J.J., van der Werf,S., Anderson,C.W. and Wimmer,E. (1981) *Nature*, **291**, 547–553.
13 Pelletier,J. and Sonenberg,N. (1988) *Nature*, **334**, 320–325.
14 Pilipenko,E.V., Blinov,V.M., Romanova,L.I., Sinyakov,A.N., Maslova,S.V. and Agol,V.I. (1989) *Virology*, **168**, 201–209.
15 Skinner,M.A., Racaniello,V.R., Dunn,G., Cooper,J., Minor,P.D. and Almond,J.W. (1989) *J. Mol. Biol.*, **207**, 379–392.
16 Le,S.Y. and Zuker,M. (1990) *J. Mol. Biol.*, **216**, 729–741.
17 Haller,A.A. and Semler,B.L. (1992) *J. Virol.*, **66**, 5075–5086.
18 Haller,A.A., Stewart,S.R. and Semler,B.L. (1996) *J. Virol.*, **70**, 1467–1474.
19 Charini,W.A., Burns,C.C., Ehrenfeld,E. and Semler,B.L. (1991) *J. Virol.*, **65**, 2655–2665.
20 Campos,R. and Villarreal,L.P. (1982) *Virology*, **119**, 1–11.
21 McMaster,G.K. and Carmichael,G.G. (1977) *Proc. Natl Acad. Sci. USA*, **74**, 4835–4838.
22 Todd,S. and Semler,B.L. (1996) *Nucleic Acids Res.*, **24**, 2133–2142.
23 Kawamura,N., Kohara,M., Abe,S., Komatsu,T., Tago,K., Arita,M. and Nomoto,A. (1989) *J. Virol.*, **63**, 1302–1309.
24 Ren,R.B., Moss,E.G. and Racaniello,V.R. (1991) *J. Virol.*, **65**, 1377–1382.